Bulletin of the Seismological Society of America, Vol. 76, No. 5, pp. 1433–1445, October 1986

MICROSEISM PROPAGATION BETWEEN TWO SITES ON THE DEEP SEAFLOOR

By Spahr C. Webb and Steven C. Constable

Abstract

Pressure and electric field fluctuations detected at two sites separated by a distance of 32 km on the deep seafloor are found to be partially coherent at frequencies between 0.05 and 0.6 Hz. The phase relationships observed between the two sites suggest coherent wave trains from three source regions produce the observed coherence. Plausible estimates for the azimuths to the sources can be obtained if Rayleigh wave phase velocities are assumed. Each source region is associated with a different peak in the power spectra of the pressure and electric field fluctuations. One source region is along the California coastline where microseisms between 0.05 and 0.1 Hz are generated by the steepening and breaking of swell along that coast. The two other source regions are in deep water where microseisms are produced by nonlinear interaction of surface gravity waves. These microseisms have frequencies which are double the frequency of principal surface gravity wave components. A region to the southeast of the two sites is associated with microseisms near 0.16 Hz, and a region to the northwest is associated with microseisms near 0.25 Hz.

Introduction

We report on measurements of pressure and electric field fluctuations from two sites separated by a distance of 32 km on the deep seafloor. A nearly continuous record of these two variables sampled at 1.6 Hz (pressure) or 0.8 Hz (electric field) was obtained over a 4-day period in September 1984 at the two sites shown in Figure 1. The pressure and electric field transducers are decribed in Cox *et al.* (1984) and in Webb *et al.* (1986), and have been used in several previous studies of microseisms and surface gravity waves (Webb and Cox, 1984, 1986).

The coherence between fluctuations at the two sites has been estimated from the observations. The coherence measurements constrain the character of the wave field associated with seafloor (microseism) noise. No coherence would be detected between distant sites if the wave field was nearly isotropic in wavenumber, but some coherence is expected if the wavenumbers are clustered on the dispersion curves corresponding to a small number of modes.

The predominant mechanism which forces microseisms acts isotropically (Hasselmann, 1963), and it is probably not unreasonable to model the microseism wave field as isotropic at frequencies above a few Hertz, as the number of modes present is probably very large. At lower frequencies, only a few modes (of surface waves) are excited (Webb and Cox, 1986) so isotropy is a poor model. We use the coherences detected at frequencies below 1 Hz to constrain the directional spectrum of the microseism wave field.

Data Analysis

The coherences and power spectra in Figures 2 to 7 were obtained from ensemble averages of Fast Fourier transforms of data records from the entire 4-day experiment (26 September 1984, 02:36 to 30 September 1984, 04:36). Each data record is one data point short of one-half hour, and each record was multiplied by a 4π prolate window before transforming. The 4π prolate window has low broad band bias (spectral leakage), important when computing spectra with large dynamic ranges, but permits rather poor resolution in frequency (Thomson, 1977).

In the figures in the second half of the paper (Figures 8 to 10), resolution in frequency has been traded off in favor of shorter data sections (to study signals which are present only temporarily) and against a larger degree of freedom (allowing better constraints on coherence estimates). The record sections have been divided

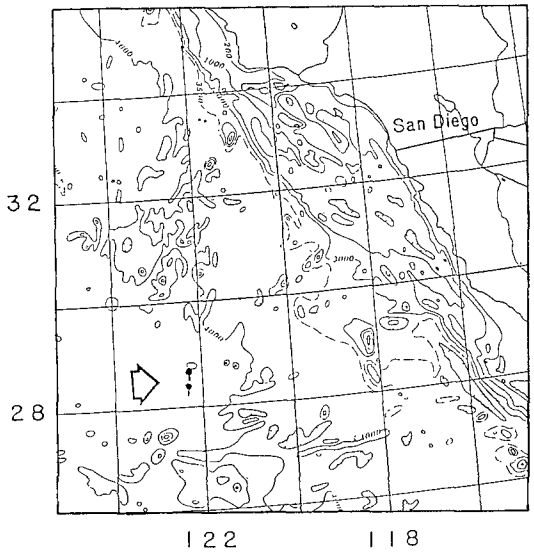

FIG. 1. An arrow points toward the two instrument sites. The orientation of the antennas is depicted by the "tails" on each point. The bathymetry is in meters with a contour interval of 500 m.

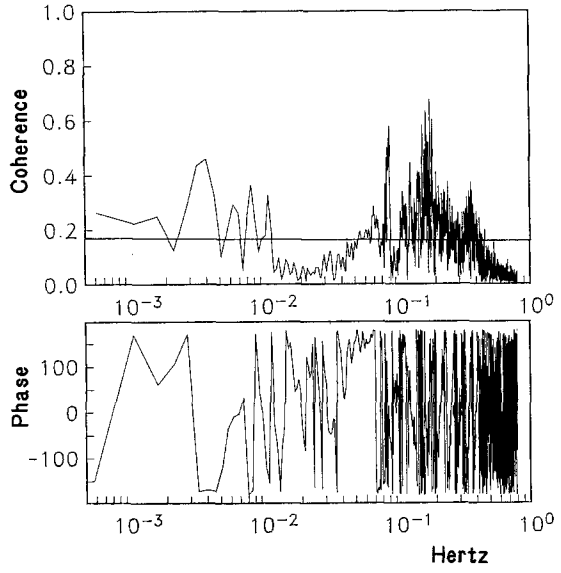

FIG. 2. The coherence and phase (in degrees) between pressure fluctuations at the two sites versus frequency. The level above which the coherence differs from zero at the 95 per cent significance level is marked with a solid line. The coherence estimate is based on 196 degrees of freedom.

into shorter data blocks, windowed with the same 4π prolate window before transforming. Because the window is such a severe taper, the data blocks can be permitted to overlap as much as 30 per cent, without the spectral estimates from overlapping blocks being significantly correlated. Overlapping the data blocks

increases the number of degrees of freedom available. This strategy of data analysis has superior rejection of broad band bias to the procedure which takes averages of the power in adjacent frequency bands from the Fourier transform of the much longer, unsectioned data set that is windowed with a much less severe taper (a 10 per cent cosine bell or no taper at all).

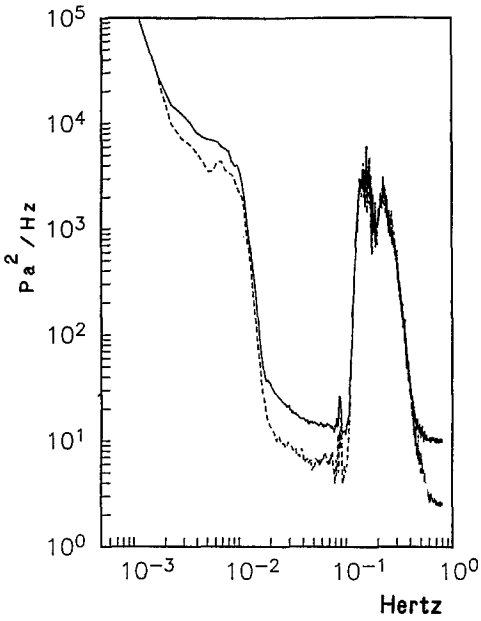

FIG. 3. Power spectra of pressure fluctuations at the northern site (solid line) and the southern site (dashed line) versus frequency (196 degrees of freedom).

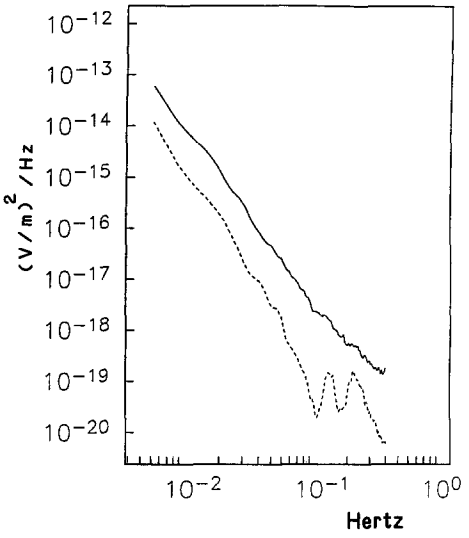

FIG. 4. Power spectra of electric field fluctuations at the northern site (solid line) and the southern site (dashed line) (692 degrees of freedom).

COHERENCES AND POWER SPECTRA

Significant coherence was found between pressure fluctuations from the two sites in two frequency bands: from 0.001 to 0.014 Hz (70- to 1000-sec period) and from 0.05 to 0.4 Hz (2.5- to 20-sec, see Figure 2). The pressure fluctuations in the lower

band are caused by surface gravity waves and are described in another paper (Webb, 1986). The pressure fluctuations in the higher frequency band are caused by Rayleigh waves (microseisms). The coherence is defined as the magnitude of the cross-spectrum divided by the square root of the product of the autospectra. The coherence

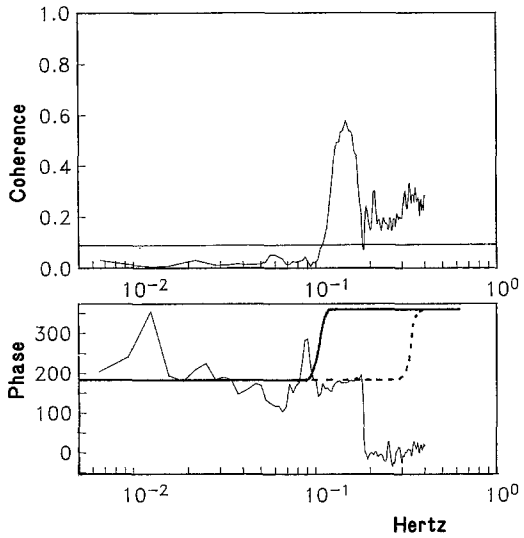

FIG. 5. (*Top*) Coherence between electric field and pressure fluctuations at the southern site versus frequency. (*Bottom*) Observed phase in degrees between pressure and the electric field fluctuations "unwrapped" to show the behavior near 180° clearly (thin line). Also plotted: predicted phase relationship between one horizontal component of the electric field and pressure fluctuations at the seafloor in a fundamental mode (heavy solid line) and second mode (dashed line) Rayleigh waves (686 degrees of freedom).

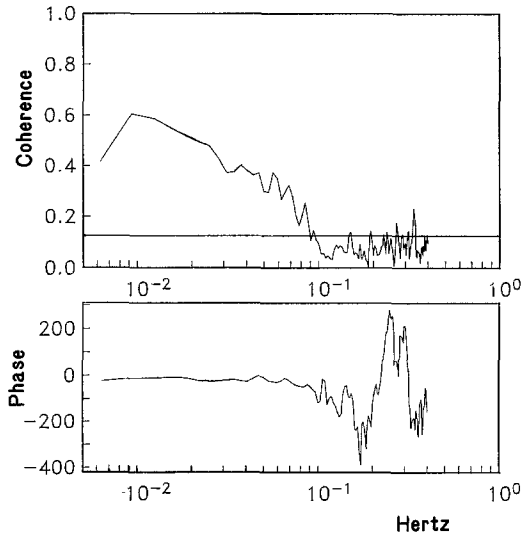

FIG. 6. Coherence and unwrapped phase between electric field fluctuations at the southern site and pressure fluctuations at the northern site (446 degrees of freedom).

plotted in Figure 2 has 196 degrees of freedom so that the coherence differs significantly from zero at the 95 per cent confidence level if the coherence exceeds 0.18.

Power spectra of the pressure fluctuations from the two sites averaged over the

4-day period are plotted in Figure 3. The two spectra are very similar; the differences apparent in the low energy bands in the spectrum are caused by instrument noise of unknown origin. Both the electric field and pressure measurements were particularly noisy during this experiment in comparison with previous measurements.

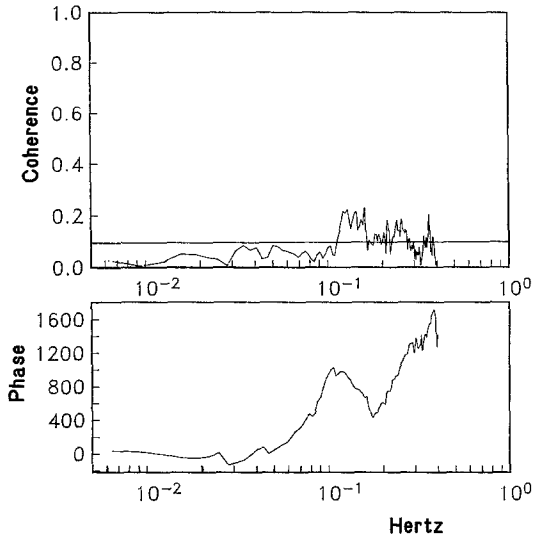

FIG. 7. Coherence and unwrapped phase between electric field fluctuations observed at the two sites (388 degrees of freedom).

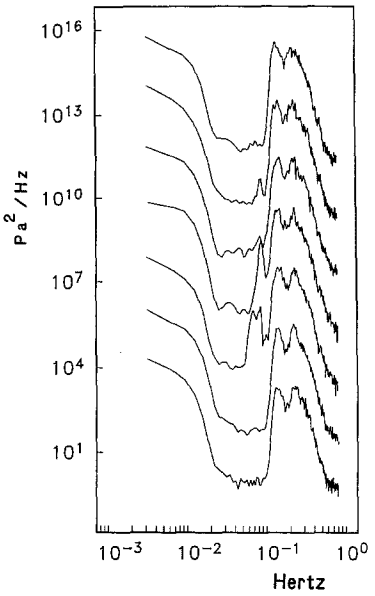

FIG. 8. A series of power spectra of pressure fluctuations observed at the northern site. Except for one-half hour gaps after the second and fourth spectra and a gap in the middle of the data set for the fifth spectrum, each spectrum is based on a 1-hr-long segment of a continuous record. Each spectrum is shifted upward two decades from the previous spectrum so that it can be seen clearly (28 degrees of freedom).

The energetic part of the spectrum below 0.02 Hz is associated with surface gravity waves and persists at the same level throughout the experiment. In contrast, the several peaks near 0.08, 0.16, and 0.25 Hz vary considerably during the course of the experiment. The peak at 0.08 Hz is only present for a few hours. Since the

microseism signals are not stationary over the entire 4-day experiment, the coherence in Figure 2 is likely to be an underestimate of the coherences in the microseism wave field.

Motion of the seafloor and sea water near the seafloor through the geomagnetic

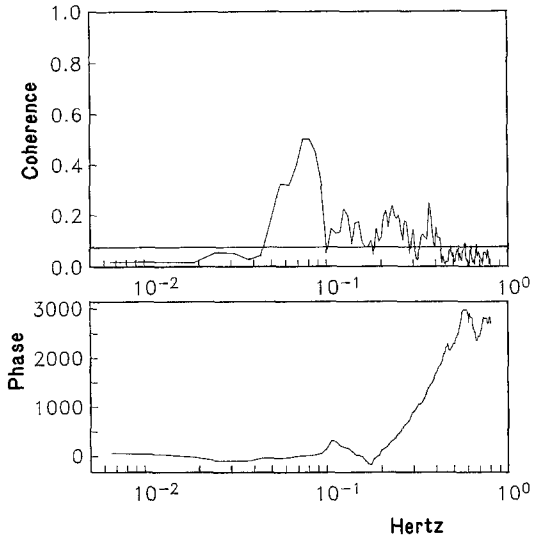

FIG. 9. Coherence and unwrapped phase between pressure fluctuations at the two sites based on data from 27 September 02:06 to 28 September 22:36 (990 degrees of freedom).

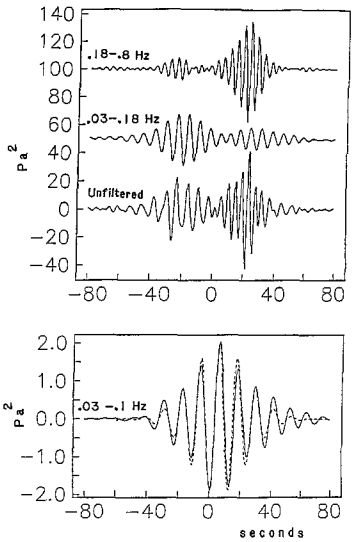

FIG. 10. The covariance between pressure fluctuations at the two sites in four frequency bands. A model for the covariance for a narrow band spectral peak is plotted dashed in the lower panel.

field induces a voltage in an antenna lying on the seafloor (Webb and Cox, 1982). The absence of any other significant source of electrical noise at the deep seafloor in the microseism band permits the small microseism signals to be detected across an antenna 600 m long, and we use the electric field signals to infer seafloor motions. At both sites, a single antenna detected motions perpendicular to the orientation of

the antenna. The approximate antenna orientations are plotted on Figure 1. The electric field transducers were deployed as part of the controlled source electromagnetic sounding experiment which is described in Cox *et al.* (1986).

A power spectrum of the electric field fluctuations from the southern site is plotted in Figure 4 (dashed line). The two microseism peaks are apparent at 0.16 and 0.25 Hz, but the lowest frequency microseism peak near 0.08 Hz is obscured by electric field signals generated by magnetospheric disturbances. The measurements from the northern site are too noisy to be useful, and again the source of noise is probably instrumental.

The electric field signal at the southern site is partially coherent with the pressure signal at the same site (Figure 5). This figure can be considered a measure of the coherence between one horizontal component of velocity perpendicular to the antenna (roughly east-west) and the pressure fluctuations. The phase hovers near 0° or 180° as is expected in Rayleigh waves. The phase in this figure has been "unwrapped" in the sense that the phase has been allowed to vary beyond ±180°, and jumps in the phase between adjacent frequency bands have been restricted to less than ±180°.

A small, but significant coherence is also detected between 0.1 and 0.25 Hz, between fluctuations in the electric field at the southern site and the pressure fluctuations at the northern site (Figure 6). At low frequencies, significant coherence is detected between the electric field at the northern site and the southern site (Figure 7), despite the high noise level in measurements from the northern site; this coherence is merely a reflection of the very large length scales associated with magnetospheric disturbances.

Microseism Generation

Two mechanisms are recognized for generating microseisms at the frequencies of the peaks seen in the pressure spectrum (Figure 3). The peak near 0.08 Hz is caused by seismic waves forced by the steepening and breaking of surface gravity waves (swell) along the coast (Hasselmann, 1963). This is a "primary" frequency peak because the seismic waves are predominantly at frequencies near the primary swell frequency. The peaks at 0.16 and 0.25 Hz are caused by seismic waves generated by nonlinear interaction of surface gravity waves in the open ocean. This mechanism was first explained by Longuet-Higgins (1950), and the theory was extended by Hasselmann (1963). The nonlinear mechanism forces seismic waves at twice the frequency of the principal surface gravity wave components, hence these are "double"-frequency peaks. Observations of Haubrich *et al.* (1963) and many others have demonstrated the relationship of seismic noise to surface gravity waves over the ocean. Recent seafloor measurements seem to confirm many of the details of Hasselmann's theory (Kibblewhite and Ewans, 1985; Webb and Cox, 1986).

Propagation at the Frequencies of the Three Peaks

The single frequency peak near 0.084 Hz is only present during a few hours of the experiment. Power spectra calculated on nearly sequential 1 hr blocks of data show the peak appearing within a 2-hr period (Figure 8). The peak drifts slowly toward slightly higher frequency over the next several hours and disappears completely after 6 hr. The reason for the ephemeral character of the peak is not known. The peak is generated by the action of swell at the coast, but the swell which generates the seismic waves does not change in amplitude or frequency during the evolution of the peak. A similar, very temporary peak was observed during a previous

seafloor experiment (Webb and Cox, 1986) but observers of single-frequency peaks at continental sites do not seem to have noted the same transience (Haubrich *et al.*, 1963; Haubrich and McCamy, 1969).

The coherence calculated on data from a 25-hr period which includes the period when the single frequency peak is present shows the coherence is high between the pressure records from the two sites at the frequencies in the peak (Figure 9). We have also calculated the coherence on an even shorter data set (2 hr) from the period when the peak at 0.08 Hz is the most energetic. The calculation reveals that the coherence in the single-frequency peak is as high as 0.92. That coherence was calculated with 120 degrees of freedom so the 95 per cent confidence limits on the estimate are at 0.89 and 0.94.

The high coherences detected are indicative of a narrow beam of waves from a localized source. The phase of the coherence increases with increasing frequency within the peak (Figure 9) and thus is consistent with a wave train of waves reaching the northern transducer before the southern transducer.

The properties of this wave train are more clearly shown in the covariance. The covariance between data series x_i and y_i at a time lag $\tau_j = \Delta t \cdot j$ is normally defined as

$$C(\tau_j) = \frac{1}{N} \sum_{i=1}^{N} (x_{i+j} - \bar{x})(y_i - \bar{y})$$

where $\bar{x}$ and $\bar{y}$ are the means of the two series. The covariance can be shown to be equal to the inverse Fourier transform of the cross spectrum. Because we normally calculate the cross-spectrum in the course of calculating the coherence, we have calculated the covariance shown in Figure 10 from the cross-spectrum. This method of calculating the covariance also allows us to filter the cross-spectrum before the forward transform is applied. This enables us to examine the contribution to the covariance of various frequency bands. Because the spectrum is quite "peaky," individual peaks can be isolated with "boxcar" filters (filter coefficients equal to one in the pass band, zero elsewhere).

Filtering the cross-spectrum to a narrow band between 0.03 and 0.1 Hz generates the covariance shown in the bottom trace of Figure 10. We model the trace by assuming a narrow band wave train traveling in a single direction. The covariance is related to the frequency spectrum $S(\omega)$ by

$$\mathrm{cov}(\tau) = \int S(\omega)\cos(\omega(x/c - \tau))\, d\omega.$$

Here, c is the phase speed; we assume it is a constant. If we model the spectrum as $S(\omega) = A \exp(-(\omega - \omega_0)^2\Delta^2/2)$ (a Gaussian or "bell"-shaped spectral peak), then the covariance is

$$\mathrm{cov}(\tau) = A \exp(-(x/c - \tau)^2/\Delta^2)\cos(x/c - \omega_0\tau),$$

which can be described as a monochromatic signal of frequency ω_0 modulated by a Gaussian curve of width Δ.

We plot in Figure 10 (dashed line) the best-fitting model (by eye) for the covariance ($\Delta = 25$ sec, $\omega_0 = 0.53$ sec^{-1} and $c = 4.5$ km/sec). Thus, the observed covariance and therefore the phase of the coherence in Figure 9 are now consistent with wave propagating from the northern instrument toward the southern instru-

ment at an apparent phase speed of 4.5 km/sec. Rayleigh waves do not normally travel as fast as 4.5 km/sec in oceanic structures at those frequencies, but travel more typically at a phase speed near 4 km/sec. Our interpretation is that waves are propagating in a direction 27° away from the line between the instruments producing a higher apparent phase speed. Either 207° or 153° is possible for the direction of propagation; we chose 207° because these waves must originate at the coast.

The coherence is considerably lower in the two double-frequency peaks at 0.16 and 0.25 Hz (roughly 0.2) than in the single-frequency peak at 0.08 Hz (Figure 9). This estimate has 990 degrees of freedom so the 95 per cent confidence interval around 0.2 is from about 0.14 to 0.26. The phase estimate in Figure 9 has a 95 per cent confidence limit of about ±17° at those frequencies for which the coherence is 0.2. The area of ocean surface over which the surface gravity waves could be interacting to generate the seismic waves detected in the single-frequency peaks is very large. In contrast, the single-frequency peak seems to be associated with a localized source. A much broader directional spectrum associated with the double-frequency peaks would be consistent with the lower coherences detected at those frequencies, as the interference of waves from slightly different directions will reduce the coherence.

The phase of the coherence in these two peaks is consistent with waves propagating from the south forming the peak at 0.16 Hz and waves propagating from the north forming the peak near 0.25 Hz. The phase decreases with increasing frequency between 0.1 and 0.18 Hz, then increases with increasing frequency from 0.18 to about 0.6 Hz. Above 0.6 Hz, the phase appears random, and the coherence is not significant. The covariance (Figure 10) also demonstrates that the waves forming the two peaks travel from two different directions, and thus are associated with two distinct source regions. The two filtered traces in the upper panel of Figure 10 show that for most of the energy at frequencies below 0.18 Hz, the signal appears first at the southern transducer, while at higher frequencies the signal at the northern transducer leads the signal at the southern transducer. The partition of energy between northward-propagating, low-frequency waves and southward-propagating, high-frequency waves is not complete, but the microseism peaks clearly overlap in frequency (Figure 3).

At the frequencies of both of these double-frequency peaks, Rayleigh waves in oceanic structures are strongly dispersive. The phase velocities of the first three Rayleigh wave modes in a model of the oceanic crust have been plotted in Figure 11 (see Webb and Cox, 1986, for details of the model). We would like to estimate the phase velocity from our measurements of the phase difference; however, we do not have a third independent measurement which would permit us to determine the direction of propagation. If we assume that the direction of propagation is the same for all waves in a given peak, then we can perform a curve fit to the dispersion curve in Figure 11 to determine the direction of propagation. The points plotted in Figure 11 indicate the phase velocities estimated from the phase differences which result when the direction of propagation is taken to be either 55° or 305°. No consistent relationship can be found at frequencies near 0.25 Hz. More than one mode can be excited at frequencies above 0.25 Hz and beating between modes would preclude a stable phase estimate. It is also likely that the directional spectrum at frequencies near 0.25 Hz is quite broad, which would make nonsense of this procedure. These questions could much better be addressed with a multi-element array of instruments.

We can resolve the ambiguity between the two azimuths (55° or 305°) estimated

for waves in the peak at 0.16 Hz by examining the phase of the electric field with respect to pressure. This is equivalent to examining the phase between the east-west component of the seafloor velocity and the pressure to determine if the waves are propagating in an easterly or westerly direction. However, the electric field-pressure phase relationship is slightly more complicated. The electric field sensed by an antenna lying on the seafloor induced by seismic waves can be approximated by $E \sim (u_s - u_w) \times F$; the vector cross-product of the seafloor velocity (u_s) minus the velocity in the sea water just above the seafloor (u_w), with the geomagnetic field (F). Webb and Cox (1982) calculate this phase relationship in the first several Rayleigh wave modes. The antenna senses a single component of E and is sensitive primarily to horizontal motions perpendicular to the orientation of the antenna. We have plotted in Figure 5 the phase relationship for the first two Rayleigh wave

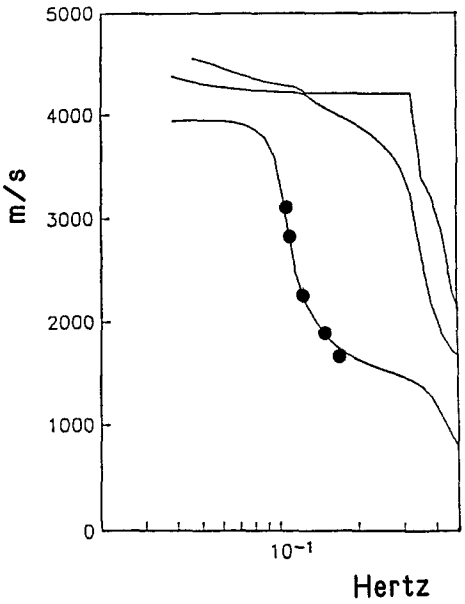

FIG. 11. Phase velocity versus frequency for the first three Rayleigh wave modes. Also plotted (large dots), the phase velocity derived from the phase delays between sites and an estimate of the propagation direction.

modes. The phase of the fundamental mode changes from 0° to 180° near 0.1 Hz. The observed phase (also plotted on Figure 5) shows the phase changing 180° from 0.16 to 0.25 Hz. Our interpretation is that the source of waves generating the double-frequency peak at 0.16 Hz is to the east of the antenna, whereas the source of the waves near 0.25 Hz is to the west of the antenna. Another possibility is that both sets of waves are coming from the east but that the waves at 0.25 Hz are of the second mode. However, Webb and Cox (1985) find that the microseism-generating mechanisms are very inefficient at generating second modes at frequencies as low as 0.25 Hz. Other seafloor observations have not seen second mode waves near 0.25 Hz (Latham and Sutton, 1966).

We note lastly that the phase of the electric field observed at the southern site with respect to the pressure at the northern site (Figure 5) is consistent with the phase observed at the same site (Figure 4) once the phase difference observed between the pressure fluctuations at the two sites (Figure 9) is taken into account.

CONCLUSIONS

We have plotted on Figure 12 a summary of our inferences about the directional spectrum of the microseism wave field. The waves forming the peak near 0.08 Hz originate at the California coast. The peak at 0.16 Hz is formed by waves originating from the southeast. The confused seas under cyclone Polo are probably the source of these microseisms, and we have plotted the position of this cyclone on the day of the coherence estimates in Figures 6 to 10 (Gunther and Cross, 1985). Cyclones are energetic sources of microseisms, and cyclones can be tracked from land stations

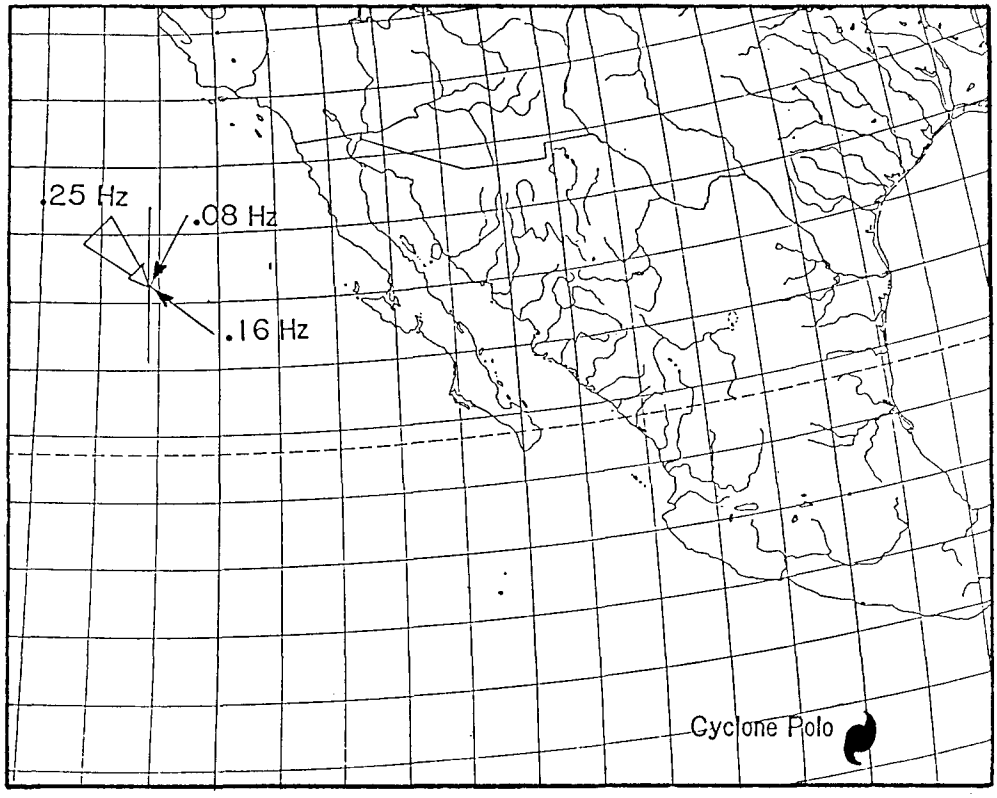

FIG. 12. Chart showing the direction of propagation of waves in the three microseism spectral peaks. The wide arrow labeled "0.25 Hz" signifies the directional spectrum is probably broad in that band and the propagation poorly known. The location of cyclone Polo on 27 September 1984 is also plotted.

using microseisms, although not very well because of scattering and refraction effects (Iyer, 1958). Finally, the peak at 0.25 Hz is probably generated over a broad region to the northwest of the sites. The winds typically found in this area off of the California coast are sufficiently strong to produce the waves with frequencies as low as 0.125 Hz which are required to generate microseisms at 0.25 Hz (Webb and Cox, 1986). The low coherence between the electric field and pressure fluctuations at the southern site (Figure 4) at 0.25 Hz when compared to the coherence at 0.16 Hz suggests the directional spectrum is much broader at higher frequencies, which also suggests a large source region.

We have produced a sketchy account of the directional spectrum of microseisms at frequencies between 0.05 and 0.6 Hz. The details of the directional spectrum are not very important. The significant finding of this study is that coherence can be

detected in the seafloor motions and the pressure fluctuations between transducers separated by tens of kilometers. As far as we know, this is the first published report of coherence detected between seismic instruments at different sites on the seafloor (ignoring earthquake waves). Presumably, the emphasis on shorter periods in other studies has precluded the possibility of finding significant coherence in the microseism wave field during typical seafloor deployments.

Significant coherence is found in microseisms between stations separated by many kilometers at continental sites. Small arrays have been used to measure the coherence and phase so as to determine phase velocity (Toksöz, 1964; Asten and Henstridge, 1984), and large arrays have been used to measure the directional spectrum of the microseism wave field as well (Toksöz and Lacoss, 1968). However, it was not apparent before this study that significant coherence would be found between seafloor sites. Microseisms can be forced by the double-frequency mechanism anywhere in the ocean. This mechanism forces waves isotropically; thus within a region of strong local forcing, the wavenumber spectrum of the microseisms wave field could be nearly isotropic, and the coherence would fall very rapidly with the distance between sites.

A small array could be used to estimate the directional spectrum and from this infer the strength of local forcing. The array could also be used to measure phase velocity. This study suggests measurements could be made in a band from about 0.05 to perhaps 0.6 Hz, although we suspect the upper and lower frequency bounds will depend on the weather and the location.

ACKNOWLEDGMENTS

The data used in this study were obtained from instruments built and deployed by the group headed by Professor Charles Cox at the Scripps Institution of Oceanography. Dr. Webb was supported as a postdoctoral scholar by the Woods Hole Oceanographic Institution while completing this work. This work was also supported by the Office of Navy Research and NORDA.

REFERENCES

Asten, M. W. and J. D. Henstridge (1984). Arrays estimators and the use of microseism for reconnaissance of sedimentary basins, *Geophysics* **49,** 829–837.

Cox, C. S., T. Deaton, and S. C. Webb (1984). A deep sea differential pressure gauge, *J. Atmos. Oceanic Technol.* **1,** 237–246.

Cox, C. S., S. C. Constable, A. D. Chave, and S. C. Webb (1986). Controlled source electromagnetic sounding of the oceanic lithosphere, *Nature* **320,** 52–54.

Gunther, E. B. and R. L. Cross (1985). Eastern North Pacific tropical cyclones, 1984, *Mariners Weather Log* **29,** 63–71.

Hasselmann, K. A. (1963). A statistical analysis of the generation of microseisms, *Rev. Geophys. Space Phys.* **1,** 177–210.

Haubrich, R. A. and R. L. McCamy (1963). Microseisms: coastal and pelagic sources, *Rev. Geophys.* **7,** 539–572.

Haubrich, R. A., W. H. Munk, and F. E. Snodgrass (1963). Comparative spectra of microseisms and swell, *Bull. Seism. Soc. Am.* **53,** 1032–1039.

Iyer, H. (1958). A study on the direction of arrival of microseisms, at Kew Observatory, *Geophys. J. R. Astr. Soc.* **1,** 32–43.

Kibblewhite, A. C. and K. C. Ewans (1985). Wave-wave interactions, microseisms and infrasonic ambient noise in the ocean, *J. Acoust. Soc. Am.* **78,** 981–994.

Latham, G. V. and G. H. Sutton (1966). Seismic measurements on the ocean floor, *J. Geophys. Res.* **71,** 2545–2573.

Longuet-Higgins, M. S. (1950. A theory of the origin of microseisms, *Phil. Trans. R. Soc. Lond., Ser. A* **243,** 1–35.

Thomson, D. J. (1977). Spectrum estimation techniques for characterization and development of the WT4 waveguide, part 1, *Bell Sys. Tech. J.* **56,** 1764–1815.

Toksöz, M. N. (1964). Microseisms and an attempted application to exploration, *Geophysics* **29,** 154–177.
Toksöz, M. N. and R. T. Lacoss (1968). Microseisms: mode structure and sources, *Science* **159,** 872–873.
Webb, S. C. (1986). Coherent pressure fluctuations observed at two sites on the deep sea floor, *Geophys. Res. Letters* **13,** 141–144.
Webb, S. C. and C. S. Cox (1982). Electromagnetic fields induced at the seafloor by Rayleigh-Stoneley waves, *J. Geophys. Res.* **87,** 4093–4102.
Webb, S. C. and C. S. Cox (1984). Pressure and electric field fluctuations on the deep sea floor: background noise for seismic detection, *Geophys. Res. Letters* **11,** 967–970.
Webb, S. C. and C. S. Cox (1986). Observations and modeling of seafloor microseisms, *J. Geophys. Res.* **91,** 7343–7358.
Webb, S. C., C. S. Constable, C. S. Cox, and T. K. Deaton (1986). A seafloor electric field instrument, *J. Geomagnet. Geoelect.* **37,** 1115–1129.

DEPARTMENT OF GEOLOGY AND GEOPHYSICS
WOODS HOLE OCEANOGRAPHIC INSTITUTION
WOODS HOLE, MASSACHUSETTS 02543 (S.C.W.)

SCRIPPS INSTITUTION OF OCEANOGRAPHY
MAIL CODE A-030
LA JOLLA, CALIFORNIA 92093 (S.C.C.)

Manuscript received 9 December 1985